and analysis of pre-miR-124a-1 and pre-miR-124a-2 double knockout or miR-124a-1, miR-124a-2 and miR-124a-3 triple knockout mice will be necessary to draw a definitive conclusion.

Although the number of cone cells was significantly reduced in *Rncr3*$^{-/-}$ mice ($P < 0.001$), rod photoreceptor cells did not seem to be significantly affected ($P > 0.65$; **Fig. 3c,d** and **Supplementary Fig. 4a**). When we expressed a pre-miR-124a-2 transgene in the developing photoreceptors of *Rncr3*$^{-/-}$ mice, the number of cone cells was increased (**Fig. 6d–i**), suggesting that rod cells and other retinal neurons compensate for miR-124a loss with pre-miR-124a-2. Previous studies of the *Dicer* conditional knockout mouse in the retina suggested that photoreceptor differentiation at late developmental stages requires miRNAs[9] and that, of the retinal cell types, photoreceptors are the most sensitive to an imbalance of miRNAs[29]. Our results suggest that miR-124a is one of the main miRNAs functioning in photoreceptor cell maturation.

In vivo miR-124a target mRNAs

Several groups identified target mRNAs of miR-124a in the CNS using translation assay and *in vivo* knockdown analysis. It was recently suggested that CREB1 and *Actl6a* (*BAF53a*) are miR-124a target mRNAs in *Aplysia* and mouse, respectively[30,31]. *Sox9* was also reported to be a miR-124a target in SVZ adult neurogenesis[6]. *Ptbp1* and *Ctdsp1* were reported to be targets of miR-124a and are involved in neuronal gene regulation in cultured cells[4,5]. The pairing mechanism between miRNA and target mRNA is well established as a Watson-Crick pairing known as the miRNA seed match (especially nucleotides 2–7)[32–34]. Furthermore, it was recently found that guanidine:uridine wobble base-pairing between miRNA seed region and mRNA interferes with targeting activity[35]. Taking advantage of recently updated database information, we re-examined reported miR-124a targets using TargetScan 5.1 and found *Lhx2*, a miR-124a target mRNA candidate in both humans and mice, as well as *Ptbp1*, and *Ctdsp1*. Although *Lhx2* or *Neurod1* were predicted to be miR-124a target mRNAs by a miR-124a overexpression experiment in *Xenopus*[27,36], precursor miRNA overexpression may mistakenly produce a phenotype as a result of an effect on the miRNA synthesis mechanism or off-target effects. In fact, we did not detect a significant change in NEUROD1 protein and *Otx2* transcript expression ($P > 0.79$; **Fig. 2i–l** and **Supplementary Fig. 5g,k,n**), both of which were affected by pre-miR-124a overexpression in the *Xenopus* study[27,36]. Here, we found that *Lhx2* is a target of miR-124a in retinal cones and in the dentate gyrus in *Rncr3*$^{-/-}$ mice (**Fig. 5** and **Supplementary Fig. 8a–d**). Furthermore, LHX2 protein localization did not overlap with *Lhx2* mRNA distribution in regions in which *Rncr3* was expressed (**Supplementary Fig. 8f–o**). These observations suggest that LHX2 protein expression is affected by miR-124a by translational inhibition. We also performed both a luciferase assay and qPCR of luciferase mRNA (**Supplementary Fig. 8c,d**). Notably, although the luciferase activity of the construct containing a miR-124a target sequence in its 3′ UTR was decreased by miR-124a expression, the level of luciferase mRNA was unchanged. Our *Lhx2* overexpression assay revealed that cell death was increased in the developing retina, suggesting that inhibition of *Lhx2* translation by miR-124a is one of the essential mechanisms for down-regulating *Lhx2* in the normal development of retinal cells (**Supplementary Fig. 12**).

Lhx2 functions as a selector gene for forebrain and eye development[37]. *Lhx2*-expressing normal dorsal telencephalon cells show a marked tendency to form aggregation clusters[24], implying that LHX2 contributes to the regionalization of the cortical hem (LHX2 negative) and the non–cortical hem hippocampal region (LHX2 positive)[24]. In the *Rncr3*$^{-/-}$ brain, elevation of LHX2 protein levels may lead to a higher density of dentate neurons by promoting cell aggregation (**Fig. 5i,j,l**). Furthermore, we observed aberrant sprouting of dentate gyrus axons, mossy fibers, into the CA3 region in the *Rncr3*$^{-/-}$ brain (**Fig. 4e–h**), and found that the LHX2 level affects axonal outgrowth in primary cultured hippocampal dentate neurons (**Figs. 5m–u** and **8f–j**). It was recently shown that commissural neurons, which express LHX2 protein, extend their axons, but fail to cross the midline in *Lhx2* and *Lhx9* double knockout mice, suggesting that *Lhx2*-defective commissural neurons do not respond well to guidance cues[38]. In contrast, in the CA3 region of the *Rncr3*$^{-/-}$ hippocampus, we hypothesize that dentate gyrus granule cells may have an axon elongation capability and may over-respond to guidance cues, resulting in the mis-sprouting of granule cells to the CA3 region. Although elevated LHX2 may induce the aberrant axonal elongation phenotype, it should be noted that increased cell density and aberrant sprouting of dentate neurons in the hippocampus have been observed in seizure-induced rats[39]. Thus, understanding the precise mechanism that underlies these phenotypes awaits future study. Taken together, our findings suggest that LHX2 protein level regulation by miR-124a is critical for dentate gyrus maturation and survival (**Supplementary Fig. 12**).

Implication of miR-124a in human diseases

In humans, pre-miR-124a-1 is located on chromosome 8p23.1. Notably, chromosomal duplication, deletion or mutation of the 8p23.1 region have been reported to be involved in cerebral development and neuropsychiatric disorders, including autism, bipolar disorder, schizophrenia, learning difficulties, epilepsy and microcephaly[2,40,41]. In individuals with temporal lobe epilepsy and model animals, aberrantly sprouting mossy fibers are often observed[42]. However, the molecular mechanisms remain unknown. We found that a substantial reduction or loss of mature miR-124a (by 60–80%) or loss of miR-124a-1 resulted in a small brain, neuronal dysfunction and aberrant axonal sprouting in the hippocampus (**Fig. 4**), suggesting that dis-regulation of the miR-124a expression level is involved in developmental neuropsychiatric disorders and temporal lobe epilepsy in humans with chromosome 8p abnormalities.

A recent study of FMRP, a protein that is involved in a fragile X syndrome and a RISC component interacting with Argonaute, suggested that miR-124a interacts with the FMRP protein, which is present at synapses[43,44]. It was recently reported that miR-124a is bound and regulated by dFMR1, a FMRP protein in *Drosophila*[45]. Another study found that miR-124a is present in sensory-motor synapses and is involved in synaptic plasticity through CREB in *Aplysia*[30]. Thus, it was suggested that miR-124a is important for synaptic function. In contrast, it should be noted that another study using rat hippocampal neurons found that mature miR-124a is not enriched in synaptosomes[46]. Further analysis will be needed to fully understand the role of miR-124a in synaptic functions.

There are three pre-miR-124a loci (pre-miR-124a-1, pre-miR-124a-2 and pre-miR-124a-3) in the mouse and human genomes. Our findings strongly suggest that *Rncr3* is the primary source of miR-124a. Production and analysis of miR-124a double and/or triple knockout mice, if the mutations are not lethal, will further clarify *in vivo* miR-124a function and target mRNAs in other parts of the CNS.

METHODS

Methods and any associated references are available in the online version of the paper at http://www.nature.com/natureneuroscience/.

Note: Supplementary information is available on the Nature Neuroscience website.

ACKNOWLEDGMENTS

We thank T. Maniatis for *RIPmiR-124a-2*, M. Kilimann for *Synapsin 1* promoter, Y. Omori, K. Terada, M. Ueno, N. Nagata, K. Aritake, Y. Oishi, T. Hamasaki, and H. Abe for critical comments and technical advice, and A. Tani, M. Kadowaki, Y. Kawakami, A. Ishimaru, H. Tsujii, T. Saioka, K. Sone, H. Abe, and S. Kennedy for technical assistance. This work was supported by Japan Science and Technology Agency (JST), Core Research for Evolutional Science and Technology (CREST), Grant-in-Aid for Scientific Research (B), Grant-in-Aid for Young Scientists (B), a Grant for Molecular Brain Science from the Ministry of Education, Culture, Sports, Science and Technology, the Takeda Science Foundation, the Uehara Memorial Foundation, the Mochida Memorial Foundation, and the Naito Foundation.

AUTHOR CONTRIBUTIONS

R.S. and T.F. designed the project. R.S., C.K., S.W., S.I. and T.F carried out the molecular and *in situ* hybridization experiments. R.S. and A.O. performed *in vivo* electroporation, virus infection and knockdown experiments in retinal and hippocampal neurons, and immunohistochemistry. S.U., T.K., M.K. and R.S. carried out the ERG experiments. R.S., Y.M. and T.F. produced the knockout and transgenic mice. R.S., R. Muramatsu and T.Y. carried out hippocampal tissue experiments. R.S., R. Matsui and D.W. produced lentivirus. R.S., Y.C. and Y.U. produced adeno-associated virus. R.S. and T.F. wrote the manuscript. T.F. supervised the project.

COMPETING FINANCIAL INTERESTS

The authors declare no competing financial interests.

Published online at http://www.nature.com/natureneuroscience/.
Reprints and permissions information is available online at http://www.nature.com/reprints/index.html.

1. Lagos-Quintana, M. *et al.* Identification of tissue-specific microRNAs from mouse. *Curr. Biol.* **12**, 735–739 (2002).
2. Tabarés-Seisdedos, R. & Rubenstein, J.L. Chromosome 8p as a potential hub for developmental neuropsychiatric disorders: implications for schizophrenia, autism and cancer. *Mol. Psychiatry* **14**, 563–589 (2009).
3. Lim, L.P. *et al.* Microarray analysis shows that some microRNAs downregulate large numbers of target mRNAs. *Nature* **433**, 769–773 (2005).
4. Visvanathan, J., Lee, S., Lee, B., Lee, J.W. & Lee, S.K. The microRNA miR-124 antagonizes the anti-neural REST/SCP1 pathway during embryonic CNS development. *Genes Dev.* **21**, 744–749 (2007).
5. Makeyev, E.V., Zhang, J., Carrasco, M.A. & Maniatis, T. The microRNA miR-124 promotes neuronal differentiation by triggering brain-specific alternative pre-mRNA splicing. *Mol. Cell* **27**, 435–448 (2007).
6. Cheng, L.C., Pastrana, E., Tavazoie, M. & Doetsch, F. miR-124 regulates adult neurogenesis in the subventricular zone stem cell niche. *Nat. Neurosci.* **12**, 399–408 (2009).
7. Cao, X., Pfaff, S.L. & Gage, F.H. A functional study of miR-124 in the developing neural tube. *Genes Dev.* **21**, 531–536 (2007).
8. De Pietri Tonelli, D. *et al.* miRNAs are essential for survival and differentiation of newborn neurons but not for expansion of neural progenitors during early neurogenesis in the mouse embryonic neocortex. *Development* **135**, 3911–3921 (2008).
9. Georgi, S.A. & Reh, T.A. Dicer is required for the transition from early to late progenitor state in the developing mouse retina. *J. Neurosci.* **30**, 4048–4061 (2010).
10. Koike, C. *et al.* TRPM1 is a component of the retinal ON bipolar cell transduction channel in the mGluR6 cascade. *Proc. Natl. Acad. Sci. USA* **107**, 332–337 (2010).
11. Blackshaw, S. *et al.* Genomic analysis of mouse retinal development. *PLoS Biol.* **2**, e247 (2004).
12. He, S. *et al.* MicroRNA-encoding long non-coding RNAs. *BMC Genomics* **9**, 236 (2008).
13. Hackler, L., Wan, J., Swaroop, A., Qian, J. & Zack, D.J. MicroRNA profile of the developing mouse retina. *Invest. Ophthalmol. Vis. Sci.* **51**, 1823–1831 (2010).
14. Ohsawa, R. & Kageyama, R. Regulation of retinal cell fate specification by multiple transcription factors. *Brain Res.* **1192**, 90–98 (2008).
15. Cepko, C.L., Austin, C.P., Yang, X., Alexiades, M. & Ezzeddine, D. Cell fate determination in the vertebrate retina. *Proc. Natl. Acad. Sci. USA* **93**, 589–595 (1996).
16. Ng, L. *et al.* A thyroid hormone receptor that is required for the development of green cone photoreceptors. *Nat. Genet.* **27**, 94–98 (2001).
17. Furukawa, T., Morrow, E.M. & Cepko, C.L. Crx, a novel otx-like homeobox gene, shows photoreceptor-specific expression and regulates photoreceptor differentiation. *Cell* **91**, 531–541 (1997).
18. Chen, S. *et al.* Crx, a novel Otx-like paired-homeodomain protein, binds to and transactivates photoreceptor cell-specific genes. *Neuron* **19**, 1017–1030 (1997).
19. Nishida, A. *et al.* Otx2 homeobox gene controls retinal photoreceptor cell fate and pineal gland development. *Nat. Neurosci.* **6**, 1255–1263 (2003).
20. Silber, J. *et al.* miR-124 and miR-137 inhibit proliferation of glioblastoma multiforme cells and induce differentiation of brain tumor stem cells. *BMC Med.* **6**, 14 (2008).
21. Côté, F., Collard, J.F. & Julien, J.P. Progressive neuronopathy in transgenic mice expressing the human neurofilament heavy gene: a mouse model of amyotrophic lateral sclerosis. *Cell* **73**, 35–46 (1993).
22. Okazaki, M.M., Evenson, D.A. & Nadler, J.V. Hippocampal mossy fiber sprouting and synapse formation after status epilepticus in rats: visualization after retrograde transport of biocytin. *J. Comp. Neurol.* **352**, 515–534 (1995).
23. Chow, R.L. & Lang, R.A. Early eye development in vertebrates. *Annu. Rev. Cell Dev. Biol.* **17**, 255–296 (2001).
24. Mangale, V.S. *et al.* Lhx2 selector activity specifies cortical identity and suppresses hippocampal organizer fate. *Science* **319**, 304–309 (2008).
25. Furukawa, A., Koike, C., Lippincott, P., Cepko, C.L. & Furukawa, T. The mouse Crx 5′-upstream transgene sequence directs cell-specific and developmentally regulated expression in retinal photoreceptor cells. *J. Neurosci.* **22**, 1640–1647 (2002).
26. Hoesche, C., Sauerwald, A., Veh, R.W., Krippl, B. & Kilimann, M.W. The 5′-flanking region of the rat synapsin I gene directs neuron-specific and developmentally regulated reporter gene expression in transgenic mice. *J. Biol. Chem.* **268**, 26494–26502 (1993).
27. Qiu, R. *et al.* The role of miR-124a in early development of the *Xenopus* eye. *Mech. Dev.* **126**, 804–816 (2009).
28. Conaco, C., Otto, S., Han, J.J. & Mandel, G. Reciprocal actions of REST and a microRNA promote neuronal identity. *Proc. Natl. Acad. Sci. USA* **103**, 2422–2427 (2006).
29. Damiani, D. *et al.* Dicer inactivation leads to progressive functional and structural degeneration of the mouse retina. *J. Neurosci.* **28**, 4878–4887 (2008).
30. Rajasethupathy, P. *et al.* Characterization of small RNAs in aplysia reveals a role for miR-124 in constraining synaptic plasticity through CREB. *Neuron* **63**, 803–817 (2009).
31. Yoo, A.S., Staahl, B.T., Chen, L. & Crabtree, G.R. MicroRNA-mediated switching of chromatin-remodeling complexes in neural development. *Nature* **460**, 642–646 (2009).
32. Friedman, R.C., Farh, K.K., Burge, C.B. & Bartel, D.P. Most mammalian mRNAs are conserved targets of microRNAs. *Genome Res.* **19**, 92–105 (2009).
33. Lewis, B.P., Burge, C.B. & Bartel, D.P. Conserved seed pairing, often flanked by adenosines, indicates that thousands of human genes are microRNA targets. *Cell* **120**, 15–20 (2005).
34. Lewis, B.P., Shih, I.H., Jones-Rhoades, M.W., Bartel, D.P. & Burge, C.B. Prediction of mammalian microRNA targets. *Cell* **115**, 787–798 (2003).
35. Doench, J.G. & Sharp, P.A. Specificity of microRNA target selection in translational repression. *Genes Dev.* **18**, 504–511 (2004).
36. Liu, K. *et al.* MiR-124 regulates early neurogenesis in the optic vesicle and forebrain, targeting NeuroD1. *Nucleic Acids Res.* **39**, 2869–2879 (2011).
37. Porter, F.D. *et al.* Lhx2, a LIM homeobox gene, is required for eye, forebrain and definitive erythrocyte development. *Development* **124**, 2935–2944 (1997).
38. Wilson, S.I., Shafer, B., Lee, K.J. & Dodd, J. A molecular program for contralateral trajectory: Rig-1 control by LIM homeodomain transcription factors. *Neuron* **59**, 413–424 (2008).
39. Holmes, G.L., Sarkisian, M., Ben-Ari, Y. & Chevassus-Au-Louis, N. Mossy fiber sprouting after recurrent seizures during early development in rats. *J. Comp. Neurol.* **404**, 537–553 (1999).
40. Baulac, S. *et al.* A novel locus for generalized epilepsy with febrile seizures plus in French families. *Arch. Neurol.* **65**, 943–951 (2008).
41. Glancy, M. *et al.* Transmitted duplication of 8p23.1–8p23.2 associated with speech delay, autism and learning difficulties. *Eur. J. Hum. Genet.* **17**, 37–43 (2009).
42. Koyama, R. & Ikegaya, Y. Mossy fiber sprouting as a potential therapeutic target for epilepsy. *Curr. Neurovasc. Res.* **1**, 3–10 (2004).
43. Weiler, I.J. *et al.* Fragile X mental retardation protein is translated near synapses in response to neurotransmitter activation. *Proc. Natl. Acad. Sci. USA* **94**, 5395–5400 (1997).
44. Edbauer, D. *et al.* Regulation of synaptic structure and function by FMRP-associated microRNAs miR-125b and miR-132. *Neuron* **65**, 373–384 (2010).
45. Xu, X.L., Li, Y., Wang, F. & Gao, F.B. The steady-state level of the nervous system–specific microRNA-124a is regulated by dFMR1 in *Drosophila*. *J. Neurosci.* **28**, 11883–11889 (2008).
46. Siegel, G. *et al.* A functional screen implicates microRNA-138-dependent regulation of the depalmitoylation enzyme APT1 in dendritic spine morphogenesis. *Nat. Cell Biol.* **11**, 705–716 (2009).

ONLINE METHODS

Animal care. All procedures conformed to the ARVO Statement for the Use of Animals in Ophthalmic and Vision Research and were approved by the Institutional Safety Committee on Recombinant DNA Experiments and the Animal Research Committee of Osaka Bioscience Institute. Mice were housed in a temperature-controlled room at 22 °C with a 12 h light/dark cycle. Fresh water and rodent diet were available at all times.

Generation of *Rncr3*$^{-/-}$ mice. We obtained *Rncr3* genomic clones from a screen of the 129/SvEv mouse genomic DNA library (Stratagene). We subcloned a 6.5-kb SalI-EcoRI fragment and a 4.4-kb SalI-SalI fragment from *Rncr3* genomic clones into a modified *pPNT* vector, and transfected the linearized targeting construct into the TC1 embryonic stem cell line. Genomic DNA from the liver was digested with BamHI or EcoRV, and hybridized with 5′ and 3′ probes, respectively.

Northern blot analysis. Northern blot analysis was performed as described previously[47]. An approximately 2.2-kb fragment (the BglII-BglII fragment) of mouse *Rncr3* cDNA (GenBank #BC096449) was used to synthesize the DNA probe.

PAGE northern for miR-124a. Total RNAs from mouse tissues were isolated by Trizol (Invitrogen). We denatured 20 μm of total RNAs in 5 mM EDTA containing formamide at 80 °C for 5 min, then separated them on 15% denaturing (7 M urea) polyacrylamide gels. RNAs were transferred to a nylon membrane (Pall Corporation Biodyne) at a constant current (3.3 mA cm^{-2}) for 35 min. The filter was baked for 1 h at 80 °C. LNA-modified anti-miR-124a (EXIQON, 20 pmol) was end-labeled with γ-^{32}P-ATP (3,000 Ci mmol^{-1}, Muromachi Yakuhin) using T4 polynucleotide kinase (Takara) and purified on spin columns (GE Healthcare Micro SpinTM G-25). The nylon filters were hybridized with the labeled probe in salmon sperm–containing hybridization solution (120 mM sodium phosphate (pH 7.2), 250 mM sodium chloride, 7% SDS (wt/vol) and 50% formamide (vol/vol) at 43 °C overnight, and washed twice with 0.1% SDS containing 2× SSC at 25 °C for 5 min. The filters were then exposed to X-ray film.

***In situ* hybridization.** *In situ* hybridization was performed as described previously[47]. Digoxigenin-labeled riboprobes were synthesized by T7, SP6, or T3 RNA polymerase using the *Rncr3* (same as the 3′ probe region in northern blots), *pri-miR-124a-2* (**Supplementary Table 1**), *Lhx2* (ref. 48, **Supplementary Table 1**), *Ngn2* (an EcoRI-*Xba*I fragment of cDNA AK143190), *Crx* or *Otx2* (ref. 19) cDNA as a template in the presence of 11-digoxigenin UTPs (Roche). For miR-124a detection, we used anti-miR-124a modified with a digoxigenin-labeled LNA probe (EXIQON).

Immunostaining. For immunohistochemistry, 14-μm retina and brain sections were washed twice in phosphate-buffered saline (PBS), and permeabilized with 0.1% Triton X-100 (wt/vol) in PBS, then incubated with PBS containing 4% donkey serum (vol/vol) for 1 h to block samples. The samples were incubated with a primary antibody (**Supplementary Table 2**) at 4 °C overnight. After PBS-washing, these samples were incubated with secondary antibodies at 25 °C for 1 h.

For whole-mount immunostaining of the retina, each retina was gently peeled off from the sclera, rinsed in PBS and fixed with 4% paraformaldehyde (wt/vol) in PBS for 2 h. The retinas were permeabilized by incubation in 0.1% Triton X-100 in PBS for 30 min. After washing in PBS, samples were blocked with 4% donkey serum and 0.02% Triton X-100 in PBS for 3 h. The retinas were then immunostained with primary antibodies to M-opsin and S-opsin (**Supplementary Table 2**) at 4 °C overnight. Reactions with secondary antibodies were performed overnight at 4 °C.

Western blot analysis. Western blot analysis was performed as described previously[47]. The membrane was incubated with mouse antibody to Flag (1:5,000, Sigma) or goat antibody to LHX2 (3:500; Abcam). The membrane was then incubated with a horseradish peroxidase–conjugated donkey antibody to mouse IgG (1:10,000, Jackson) or rabbit antibody to goat IgG (1:10,000, Zymed). For secondary immunoreaction, the PVDF membrane was incubated with WB Stripping Solution (Nacalai Tesque) to remove antibodies, and blocked again with 5% skim milk (wt/vol) in TBS. Further immunoblots were performed using rat antibody to GFP (1:2,000, Nacalai Tesque) or mouse antibody to β-actin (ACTB, 1:5,000, Sigma). The signals were measured using ImageJ (US National Institutes of Health).

ERG. Electroretinographic recordings were performed as described in detail[47]. In brief, ERGs were picked-up with a gold-wire loop electrode placed on the cornea. The mice were placed in a Ganzfeld bowl and stimulated with four levels of stroboscopic stimuli ranging from −5.0 to 1.0 log cd s m^{-2} to elicit scotopic ERGs, and four levels of stimuli ranging from −0.5 to 1.0 log cd s m^{-2} for the photopic ERGs. The photopic ERGs were recorded on a rod-suppressing white background of 1.3 log cd m^{-2}.

Plasmid constructs. The *Lhx2* cDNA fragment was amplified by PCR (**Supplementary Table 1**) using PrimeStar (Takara), and cloned into the *pGEM-TEasy* vector (Promega). *Lhx2* 3′ UTR–containing fragments were also amplified and cloned into *pGEM-TEasy*. Mutations in the seed match region were introduced by PCR primers (**Supplementary Table 1**). The fragments of *Lhx2* cDNA and *Lhx2* 3′ UTR were ligated into the *pCAGGS* vector. To perform the luciferase assay, we constructed a miR-124a expression plasmid. Pre-miR-124-1, pre-miR-124-2 and pre-miR-124-3 were amplified by PCR (**Supplementary Table 1**) using ExTaq polymerase (Takara), and each PCR-amplified fragment was cloned into *pCRII* plasmids (Invitrogen). After verifying the sequence, we subcloned them into *pBAsi-mU6* (Takara). The *Lhx2* 3′ UTR were ligated into *pmirGLO* (Promega) to generate *pmirGLO-Lhx2-Nat* and *pmirGLO-Lhx2-Mut*. For *Lhx2* knockdown, *pBAsi-mU6* was used for DNA vector–based shRNA synthesis. Three target sequences, shLhx2-1, shLhx2-2 and shLhx2-3 (**Supplementary Table 1**), were selected from different positions in the mouse *Lhx2* open reading frame and subcloned into the *pBAsi-mU6* vector. The inhibition abilities of shLhx2-1, shLhx2-2 and shLhx2-3 were tested by western blot analysis using cultured cells (**Supplementary Fig. 11a,b**). The strongest inhibitor of Lhx2, shLhx2-3, was used.

Generation of miR-124a-2 transgenic mice. The *pCrx2k-Cre* plasmid[19] was digested with XhoI and BamHI to remove the *Cre* gene (*pCrx2k*). *RIP-miR-124a-2* (a gift from T. Maniatis, Harvard University)[5] is a pre-miR-124a-2 expression vector that encodes pre-miR-124a-2 in an intron of the *Ds-Red* gene. We digested *RIP-miR-124a-2* and ligated it into the *pCrx2k* plasmid (*pCrx2k-Ds-Red-124a-2*; **Supplementary Fig. 9a**). To construct a transgene vector of miR-124a-2 to rescue the hippocampal phenotype, we ligated the *pUC18-4.3Syn-CAT* plasmid (a gift from M. Kilimann, Ruhr-Universität Bochum)[26] containing a rat 4.3-kb *Syn1* promoter into Ds-red-124a-2 (*pSynI4.3k-Ds-Red-124a-2*; **Supplementary Fig. 10a**). The purified construct was injected into the pronuclei of fertilized one-cell eggs of B6C3F1 mice (Oriental Bio Service) followed by implantation into pseudopregnant foster mothers (ICR mice, Japan SLC).

Luciferase assay. We transfected 0.5 μg of the reporter plasmid DNA (*pmirGLO, pmirGLO-Lhx2-3′ UTR-Nat* or *pmirGLO-Lhx2-3′ UTR-Mut*) and 2 μg of miR-124a expression vector DNA (*pBAsi-mU6, pBAsi-mU6-pre-miR-124a-1, pBAsi-mU6-pre-miR-124a-2* or *pBAsi-mU6-pre-miR-124a-3*) per well into HEK 293T cells in a 6-well plate using the calcium phosphate method. After transfection, the cells were incubated for 48 h and lysed with Reporter Lysis Buffer (Promega). P0 hippocampal cells (approximately 2 × 10^5) were transfected with *pmirGLO-Lhx2-3′ UTR-Nat*, or *pBAsi-mU6-pre-miR-124a-1-Mut* (250 ng each) by electroporation (Amaxa Nucleofector). After transfection, the cells were incubated for 72 h, washed with PBS, and lysed with Reporter Lysis Buffer. The lysates were used for luciferase assays. Luciferase activity was measured with the Dual-Glo Luciferase Assay System (Promega) according to the manufacturer's protocol using a Wallac 1420 Multilabel Counter (Wallac). Firefly luciferase activities were determined by three independent transfections and normalized by comparison with the Renilla luciferase activities of the internal control.

***In vivo* electroporation.** *In vivo* electroporation was performed on the P0 mouse retina as described previously[47]. The *pCAGGS, pCAGGS-Lhx2-Nat* or *pCAGGS-Lhx2-Mut* vectors were co-electroporated with the *pCAGGS-EGFP* vector. We used *pCAGGS* vector concentrations of 0, 2 and 3 μg μl^{-1}, *pCAGGS-Lhx2* (native or mutated) concentrations of 4, 2 and 1 μg μl^{-1}, and a *pCAGGS-EGFP* concentration of 1 μg μl^{-1} to make a 5 μg μl^{-1} DNA solution mix. The electroporated retinas were harvested at P4.

TUNEL assay. Fresh frozen retinas were sectioned to a thickness of 14 μm and fixed with 4% paraformaldehyde in PBS for 1 min. The TUNEL assay was performed according to the manufacturer's protocols.

RT-PCR and qPCR analysis. Total RNA was extracted Trizol reagent (Invitrogen), and reverse transcribed into cDNA using SuperScript II reverse transcriptase (Invitrogen) with random hexamers. Quantitative PCR was performed using a SYBR GreenER qPCR SuperMix Universal (Invitrogen). Nucleotide sequences of primers are shown in **Supplementary Table 1**. To detect mature miR-124a, we isolated total RNA using the miRNeasy Mini Kit (Qiagen), and reverse transcribed using the miScript Reverse Transcription Kit (Qiagen). Real-time qRT-PCR was performed using the miScript SYBR Green PCR kit with miScript Universal primer and the miScript Primer assay (Qiagen). For the pri-miR-124a expression assay, total RNA isolated using the miRNeasy Mini Kit was reverse transcribed to cDNA using the TaqMan reverse transcription reagent kit and following the manufacturer's protocol (Applied Biosystems). Real-time qRT-PCR was performed using TaqMan Universal PCR Master Mix and specific TaqMan Pri-miRNA Assays for *Mus musculus* miR-124-1, miR-124-2 and miR-124-3 (Applied Biosystems).

Behavior test. *Rncr3*$^{-/-}$ and wild-type mice (4–5 months old) were suspended by their tails for 3 min, and clasping duration time was measured.

Timm staining and Nissl staining. Coronal sections, 14 μm thick, from P10 frozen mouse brains were stained by the neo-Timm's method[49]. After washing in de-ionized water, sections were counterstained by 0.1%(w/v) cresyl violet (wt/vol) for 5 min, washed in 100% ethanol, and incubated in xylene. Slides were coverslipped with Permount (Fisher Scientific).

Axon outgrowth assay. Neurons from P0 mouse hippocampus were dissociated using Nerve Cell Dissociation Medium (SUMILON) according to the manufacturer's protocol. The hippocampal cells (the approximate numbers are 4×10^5) were transfected with *pCAGGS*, *pCAGGS–Lhx2-Nat* or *pCAGGS–Lhx2-Mut* (250 ng each) together with the transfected cell marker plasmid, 125 ng of *pCAGGS-FGFP* by electroporation (Amaxa Nucleofector). Then, cells were cultured on 3.5-cm poly-D-lysine–coated dishes in Nerve-Cell Culture Medium (SUMILON). For Lhx2 knockdown experiments, hippocampal cells (the approximate numbers are 2×10^5) were transfected with *pBAsi-shControl*[50] or *pBAsi–shLhx2-3* (250 ng each), together with a transfected cell marker plasmid, *pCAGGS-FGFP*. At 72 h, the cells were fixed with 4% paraformaldehyde, 4% sucrose (wt/vol), and 0.02% Triton X-100 in PBS for 30 min, then washed with PBS. After blocking with 4% donkey serum in PBS, cells were incubated with primary antibodies to PROX1 and EGFP (**Supplementary Table 2**). Following PBS washes, Alexa 488–conjugated antibody to rat IgG and Cy3-conjugated antibody to rabbit IgG were used as secondary antibodies. Images of these cells were obtained using a confocal microscope LSM700 (Zeiss), and PROX1-positive axons (longest neurite) were measured using the LSM image browser (Zeiss).

Hippocampal slice culture. A P6 SD rat brain was dissected and sliced (300 μm thick). The hippocampal slices were placed onto membranes of Millicell-CM culture inserts (Millipore) and infected with *Camk2a* promoter–driven *Lhx2-IRES-mCherry* or *mock (control)-IRES-mCherry* expression lentivirus (approximately 10^{10} PFU ml^{-1} titer) into three loci of the dentate molecular layer using a micromanipulator. Nutrition medium was composed of 25% heat-inactivated horse serum, 25% Hank's balanced salt solution, and 50% MEM. The medium was changed every 2 d. After 5 DIV, the cultured slice was fixed with 4% paraformaldehyde, 4% sucrose and 0.02% Triton X-100 in PBS for 3 h, then permeabilized with PBS, and 0.1% Triton X-100 for 30 min. The sliced section was further immunostained.

Retinal explant culture and AAV infection. The P0 eyes were enucleated, and the choroid, sclera and cornea were removed. The eyecups (retinas with lens and vitreous) were incubated with fresh DMEM/F12 media containing AAV5 (approximately 1×10^{12} particles per ml titer), which bicistronically expresses *shControl* or *shLhx2* driven by the *U6* promoter and *mCherry* driven by the *CMV* promoter (*U6-shControl-CMV-mCherry* or *U6-shLhx2- CMV-mCherry*) for 1 h at 25 °C. The lens and vitreous were removed, and the retinas were explanted with the photoreceptor side up. After a 30-min incubation, 5 μl of AAV5 vector (approximately 1×10^{12} particles) was dropped to cover the surface of the explants. The explants cultured for 5 d were immunostained with an antibody to S-opsin.

Statistical analysis. Statistical comparison of datasets were performed with Student's *t*-test. For multiple comparison, we performed one-way ANOVA with Tukey-Kramer test or Kruskal-Wallis non-parametric ANOVA with Steel-Dwass multiple comparison test. Complete statistical information is described in the **Supplementary Statistical Analysis**.

47. Sanuki, R., Omori, Y., Koike, C., Sato, S. & Furukawa, T. Panky, a novel photoreceptor-specific ankyrin repeat protein, is a transcriptional cofactor that suppresses CRX-regulated photoreceptor genes. *FEBS Lett.* **584**, 753–758 (2010).
48. Gray, P.A. *et al.* Mouse brain organization revealed through direct genome-scale TF expression analysis. *Science* **306**, 2255–2257 (2004).
49. Babb, T.L., Kupfer, W.R., Pretorius, J.K., Crandall, P.H. & Levesque, M.F. Synaptic reorganization by mossy fibers in human epileptic fascia dentata. *Neuroscience* **42**, 351–363 (1991).
50. Onishi, A. *et al.* Pias3-dependent SUMOylation directs rod photoreceptor development. *Neuron* **61**, 234–246 (2009).

doi:10.1038/nn.2897

CHANGES IN AREAS OF CAPILLARY NONPERFUSION AFTER INTRAVITREAL INJECTION OF BEVACIZUMAB IN EYES WITH BRANCH RETINAL VEIN OCCLUSION

TAKAYUKI TERUI, MD,* MINEO KONDO, MD, PHD,* TADASU SUGITA, MD, PHD,* YASUKI ITO, MD, PHD,* NAGAKO KONDO, MD, PHD,† ICHIRO OTA, MD, PHD,† KENSAKU MIYAKE, MD, PHD,† HIROKO TERASAKI, MD, PHD*

Purpose: To study the effect of an intravitreal bevacizumab (IVB) on the retinal ischemia in eyes with a branch retinal vein occlusion.

Methods: Fluorescein angiography was performed before and 1 month after the IVB (1.25 mg/0.05 mL) in 58 consecutive eyes of 58 patients with macular edema secondary to a branch retinal vein occlusion. The area of capillary nonperfusion was measured on an early-phase fluorescein angiography image by an area measurement program, and the area was expressed relative to the optic disk area (DA). A blockage of the fluorescence by the retinal hemorrhage was distinguished from nonperfusion by comparisons with retinal photographs.

Results: Thirty-seven of 58 eyes did not have any capillary nonperfusion before the IVB, and capillary nonperfusion developed in 3 of these 37 eyes 1 month after the IVB. The area of nonperfusion in these 3 eyes was 0.13, 0.47, and 0.60 DA. Twenty-one of the 58 eyes had capillary nonperfusion before the IVB, and the mean (±SD) area of nonperfusion was 3.45 ± 4.66 DA before the IVB and 3.45 ± 5.19 DA 1 month after the IVB. This change was not significant ($P = 0.36$). An increase in the area of capillary nonperfusion of >1.0 DA after the IVB was seen in only 1 of all 58 eyes.

Conclusion: These results suggest that the incidence of a significant increase in the area of capillary nonperfusion (>1 DA) during the 1 month after the IVB is very low in eyes with branch retinal vein occlusion.

RETINA 31:1068–1074, 2011

Vascular endothelial growth factor (VEGF) is one of the most important molecules in the pathogenesis of abnormal vessel permeability and growth in the eye.[1–8] Increased VEGF levels have been reported in eyes with various retinal diseases, including diabetic retinopathy,[9–11] retinopathy of prematurity,[12–14] retinal vein occlusion,[15–17] and exudative age-related macular degeneration.[18,19] Recently, several anti-VEGF agents have become available for intraocular use, and the use of these agents has revolutionized the treatment of these retinal diseases.[20,21] Of all these intravitreal anti-VEGF agents, bevacizumab (Avastin, Roche Pharma, Reinach, Switzerland), a full-length humanized monoclonal antibody of VEGF, is one of the most widely used drugs.

Although clinical trials and case reports have proven the clinical usefulness of intravitreal anti-VEGF agents in various retinal diseases,[22–27] there are several unsolved issues. One of the major controversies is whether this treatment would increase retinal ischemia

From the *Department of Ophthalmology, Nagoya University Graduate School of Medicine, Nagoya, Japan; and †Miyake Eye Hospital, Nagoya, Japan.

Supported by grants-in aid 18591913 (to M.K.), 19500416 (to Y.I.), and 18390466 (to H.T.) from the Ministry of Education, Culture, Sports, Science, and Technology, Japan.

The authors have no proprietary or conflicts of interest to disclose.

Reprint requests: Mineo Kondo, MD, PhD, Department of Ophthalmology, Nagoya University Graduate School of Medicine, 65 Tsuruma-cho, Showa-ku, Nagoya 466-8550, Japan; e-mail: kondomi@med.nagoya-u.ac.jp

because the systemic use of bevacizumab is known to increase the risk of thromboembolic events, including strokes.[28] Although there are several studies that reported that intravitreal bevacizumab (IVB) did not exacerbate retinal ischemia,[29–31] some recent clinical and experimental studies suggested that IVB may worsen ischemic changes in normal and diseased retinas.[32–37]

A search of PubMed did not extract any studies that measured the area of capillary nonperfusion before and after the IVB therapy in patients with branch retinal vein occlusion (BRVO). We hypothesized that if the IVB worsened the retinal ischemia in BRVO, then the area of capillary nonperfusion would increase within a relatively short period. Thus, the purpose of this study was to compare the area of capillary nonperfusion quantitatively before and 1 month after the IVB in eyes with macular edema secondary to BRVO.

Subjects and Methods

Subjects

To study the effect of IVB on the retinal ischemia in eyes with a BRVO, fluorescein angiography (FA) was performed before and 1 month after the IVB for all patients with BRVO who received IVB therapy at the Miyake Eye Hospital from October 2006 to November 2009. We reviewed all the FA results. The eyes that had undergone other treatments, that is, vitrectomy, laser treatments, or other drug injections, before the IVB were excluded. In the end, the FA results of 58 eyes from 58 patients were studied.

The procedures used conformed to the tenets of the Declaration of Helsinki of the World Medical Association. An informed consent had been obtained from each of the patients after they were provided sufficient information in both oral and written forms on the procedures to be used. Information on off-label use of bevacizumab was also given to all subjects.

Bevacizumab Injections

The IVB was performed in an operating room under sterile conditions. The eyes were anesthetized with 1% tetracaine eyedrops, and the fornices of the eyes were irrigated with 10% povidone–iodine. Each patient received an intravitreal injection of 1.25 mg/0.05 mL of bevacizumab using a 30-gauge needle inserted 3.5 mm from the limbus. The patient's light perception was confirmed immediately after the injection. Antibiotic drops were given for 3 days after the injection.

Fluorescein Angiography and Measurement of Capillary Nonperfusion Area

Fluorescein angiograms were recorded using a high-resolution digital fundus camera (TRC-50DX; Topcon Corporation, Tokyo, Japan) before and 1 month after the initial IVB. A series of digital images was taken after the rapid intravenous injection of 5 mL of a 10% solution of fluorescein. The fundus image subtended an angle of 60° (diameter), and the optical resolution of the digital image was 2144 ×1424 pixels for fundus photograph and 1392 ×1040 pixels for FA. One digital image in the early phase of the macular area with the fovea located at the center was used for the analyses.

Capillary nonperfusion in the peripheral retina, that is, outside the central image, was not analyzed because it was difficult to measure the exact area of peripheral nonperfusion with this system. The area of capillary nonperfusion was measured using the area measurement program of a high-resolution digital system (IMAGEnet 1024 System; Topcon Corporation; Figure 1). The area of capillary nonperfusion was defined as the area where a dropout of the retinal capillary bed was detected in the FA image.[38] A blockage of the fluorescence by the retinal hemorrhage was distinguished from the nonperfusion by comparing the FA image with retinal photographs. The measurements were performed by a retina specialist (T.T.).

Visual Acuity and Foveal Thickness

The best-corrected visual acuity was measured by a standard Japanese decimal visual acuity chart at 5 m. The decimal values were converted to the logarithm of the minimum angle of resolution (logMAR) units for statistical analyses.

The foveal thickness was determined by the optical coherence tomography (Stratus model 3000; Carl Zeiss Meditec, Dublin, CA) with software version 4.0.1. After the patients' pupils were fully dilated with 0.5% tropicamide and 0.5% phenylephrine (Mydrin-P, Santen Co, Osaka, Japan), vertical and horizontal scans of 6 mm length were imaged through the fixation point. The average foveal thickness of the vertical and horizontal scans was defined as the foveal thickness. We used this manual method to measure the foveal thickness[39,40] because it has been reported that the automatic measurement of the macular thickness often fails to identify the outer border of the neural retina.[41]

Statistical Analyses

The significance of the differences in the logMAR visual acuity, foveal thickness, and the area of capillary nonperfusion between before and 1 month

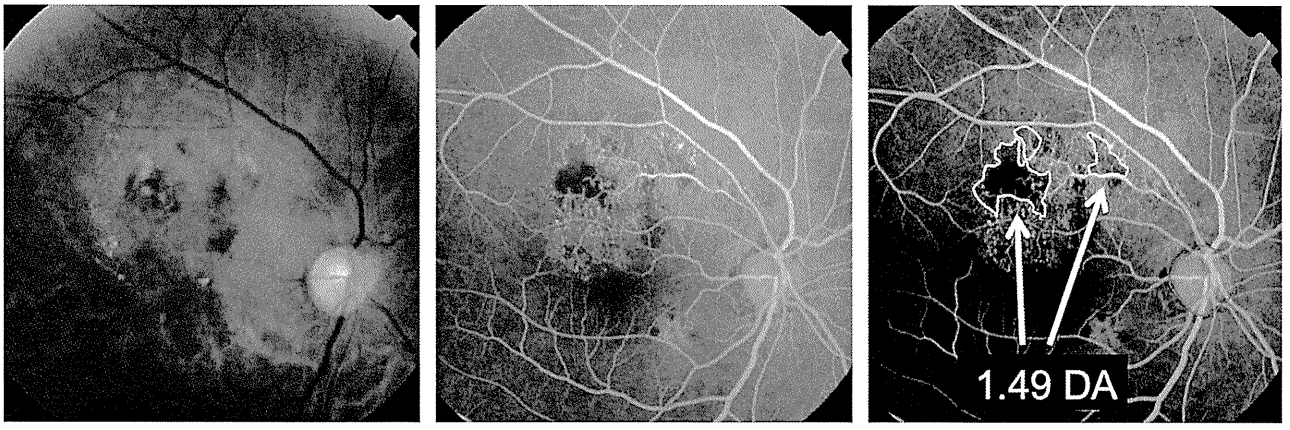

Fig. 1. Measurement of capillary nonperfusion area in a retina with BRVO. Fundus photograph (**A**) and FAs (**B** and **C**) are shown. The area of capillary nonperfusion is outlined by the use of the area measurement program of a high-resolution digital system. Blocked fluorescence lesions because of retinal hemorrhages were distinguished from nonperfusion by comparing the FA and fundus images. The area of nonperfusion is expressed relative to the DA.

after the IVB was analyzed by nonparametric Wilcoxon signed rank tests. The SPSS version 17.0J for Windows (SPSS, Inc, Chicago, IL) was used for statistical analyses. A P value of <0.05 was considered significant.

Results

Clinical Characteristics of Patients

The clinical characteristics of the 58 patients (25 men and 33 women) are summarized in Table 1. The mean age of the patients was 66.2 years (range, 41–89 years). Twenty-eight patients had systemic hypertension, 3 patients had diabetes mellitus without diabetic retinopathy, and 5 patients had hypercholesterolemia. The mean duration of the ocular symptoms before treatment was 11.0 weeks (range, 2–59 weeks).

Table 1. Baseline Clinical Characteristics of 58 Patients with Macular Edema Secondary to BRVO

Age, mean ± SD (range), years	66.2 ± 9.9 (41 to 89)
Sex	
Male/female	25/33
Period from the symptom onset to treatment, mean ± SD (range), weeks	11.0 ± 10.1 (2 to 59)
Systemic diseases	
Hypertension	28
Diabetes mellitus	3
Hypercholesterolemia	5
Visual acuity, mean ± SD (range), logMAR	0.56 ± 0.43 (−0.08 to 1.70)
Foveal thickness, mean ± SD (range), μm	565 ± 288 (155 to 1,641)

Thirty-six eyes (62.1%) had the initial IVB within 12 weeks after the onset of the symptoms.

Visual Acuity and Foveal Thickness

The mean (±SD) baseline visual acuity was 0.56 ± 0.43 logMAR units (20/69, Snellen equivalent), which significantly improved to 0.34 ± 0.37 logMAR units (20/43, Snellen equivalent) at 1 month after the IVB ($P > 0.0001$). Twenty-five of 58 eyes (43.1%) showed an improvement in visual acuity of ≥0.2 logMAR units. In contrast, only 1 eye (1.7%) showed a decrease in visual acuity of ≥0.2 logMAR units.

The mean baseline foveal thickness was 565 ± 288 μm, which significantly reduced to 256 ± 140 μm at 1 month after the treatment ($P < 0.0001$). Forty-five eyes (77.6%) showed a decrease of ≥30% in foveal thickness. Only 1 eye (1.7%) showed an increase of ≥30% in foveal thickness at 1 month after the treatment.

Changes in Area of Capillary Nonperfusion

Thirty-seven of 58 eyes did not have any capillary nonperfusion before the IVB, but new nonperfusion areas developed in 3 of these 37 eyes 1 month after the IVB. The area of nonperfusion for these 3 eyes was 0.13, 0.47, and 0.60 disk area (DA), respectively. None of these 37 eyes had an area of nonperfusion of >1.0 DA 1 month after the IVB.

Twenty-one of the 58 eyes had an area of capillary nonperfusion before the IVB, and the mean (±SD) area of nonperfusion was 3.45 ± 4.66 DA. One month after the IVB, the mean area of nonperfusion was 3.45 ± 5.19 DA. This difference was not statistically significant ($P = 0.36$). Four of these 21 eyes showed

a decrease in the area of capillary nonperfusion of >1.0 DA 1 month after the IVB (Patients 3, 13, 26, and 47, blue lines, Figure 2). However, only 1 eye showed an increase in the area of capillary nonperfusion of >1.0 DA 1 month after the IVB (Patient 23, red line, Figure 2).

Fundus photographs and FAs before and 1 month after IVB for 2 eyes are shown in Figures 3 and 4. The results from 1 eye of a 61-year-old man (Patient 47) in whom the area of capillary nonperfusion decreased from 12.49 DA to 9.52 DA 1 month after the IVB are shown in Figure 3. The best-corrected visual acuity before the IVB was 0.5 logMAR and improved to 0.7 logMAR 1 month after the IVB. In contrast, the results of 1 eye of a 62-year-old woman (Patient 23) in whom multiple soft exudates appeared in the fundus photograph and the area of capillary nonperfusion increased from 3.01 DA to 18.00 DA 1 month after the IVB are shown in Figure 4. The best-corrected visual acuity before the IVB was 0.8 logMAR and improved to 1.0 logMAR 1 month after the IVB.

Discussion

Our results demonstrated that the incidence of an increase in the area of capillary nonperfusion of >1.0 DA 1 month after the IVB therapy was very low in only 1 of 58 eyes (1.7%) in patients with macular edema secondary to BRVO. In addition, the difference in the area of nonperfusion before and 1 month after the IVB for 21 eyes that had nonperfusion before the treatment was not statistically significant ($P = 0.36$). These results suggest that a single IVB injection does not worsen the retinal ischemia in eyes with BRVO.

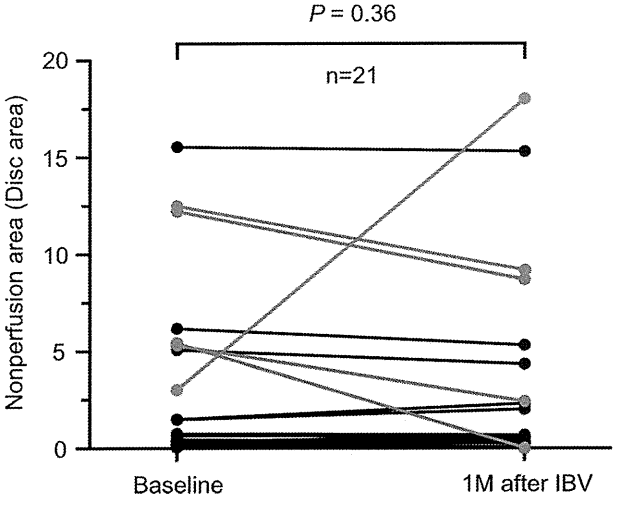

Fig. 2. Scatter plot for the area of capillary nonperfusion before and 1 month after IVB in patients with BRVO. Results from 21 patients who had capillary nonperfusion before the IVB are shown. There was no significant difference before and after the IVB in the area of nonperfusion ($P = 0.36$). Red line shows 1 eye whose nonperfusion area increased >1.0 DA after the IVB. Blue lines show 4 eyes whose nonperfusion area decreased >1.0 DA after the IVB.

Only 1 eye (Patient 23) showed a significant increase in the area of nonperfusion, namely, from 3.01 DA to 18.0 DA. This eye also developed multiple cotton wool spots (Figure 4), indicating a progression of retinal ischemia during the 1 month after the IVB therapy. However, it is uncertain whether these ischemic changes were truly related to the IVB. The patient was a 62-year-old woman with hypertension who had received the IVB very early after the onset of symptoms (2 weeks). It is known that the eyes with the nonischemic type of retinal vein occlusion often convert to ischemic type within 6 months after the onset.[42,43]

Three articles have been recently published that support our results.[29–31] Prager et al[29] followed 29 eyes with retinal vein occlusion after the IVB therapy, and while they did not measure the nonperfusion area quantitatively, they stated that there was no progression of the nonperfusion area in the FA images for all eyes. Kook et al[30] measured the degree of macular ischemia, that is, the diameter of the foveal avascular zone, before and after IVB therapy in 126 patients with chronic diabetic macular edema and reported that there was no significant change in the degree of macular ischemia. In addition, Neubauer et al[31] performed semiquantitative measurements of the nonperfused retina using an ultra wide-field scanning laser ophthalmoscope before and 1 month after IVB in 19 eyes with diabetic retinopathy. They found that the mean area of the peripheral ischemia decreased significantly 1 month after the IVB therapy. They suggested that IVB therapy may improve the peripheral retinal ischemia in the short term.

Contrary to these reports, other authors suggested that the IVB therapy may worsen retinal ischemia. Papadopoulou et al[32] reported that the diameter of the retinal arterioles significantly decreased after an intravitreal injection of ranibizumab (Lucentis, Novartis Pharma, Basel, Switzerland), a high-affinity, humanized, recombinant, antigen-binding fragment in patients with age-related macular degeneration. They suggested that intravitreal anti-VEGF agents may cause retinal circulatory disturbances. Although they reported a decrease in the vessel diameter after the injection of anti-VEGF agents, they did not show any progression of retinal ischemia associated with vasoconstriction by ranibizumab.

Ameri et al[33] evaluated the effects of IVB in a rabbit retinal neovascularization model produced by an intravitreal injection of VEGF. They observed the development of severe capillary nonperfusion in 4 of 5 rabbits in which the bevacizumab was injected 1 week

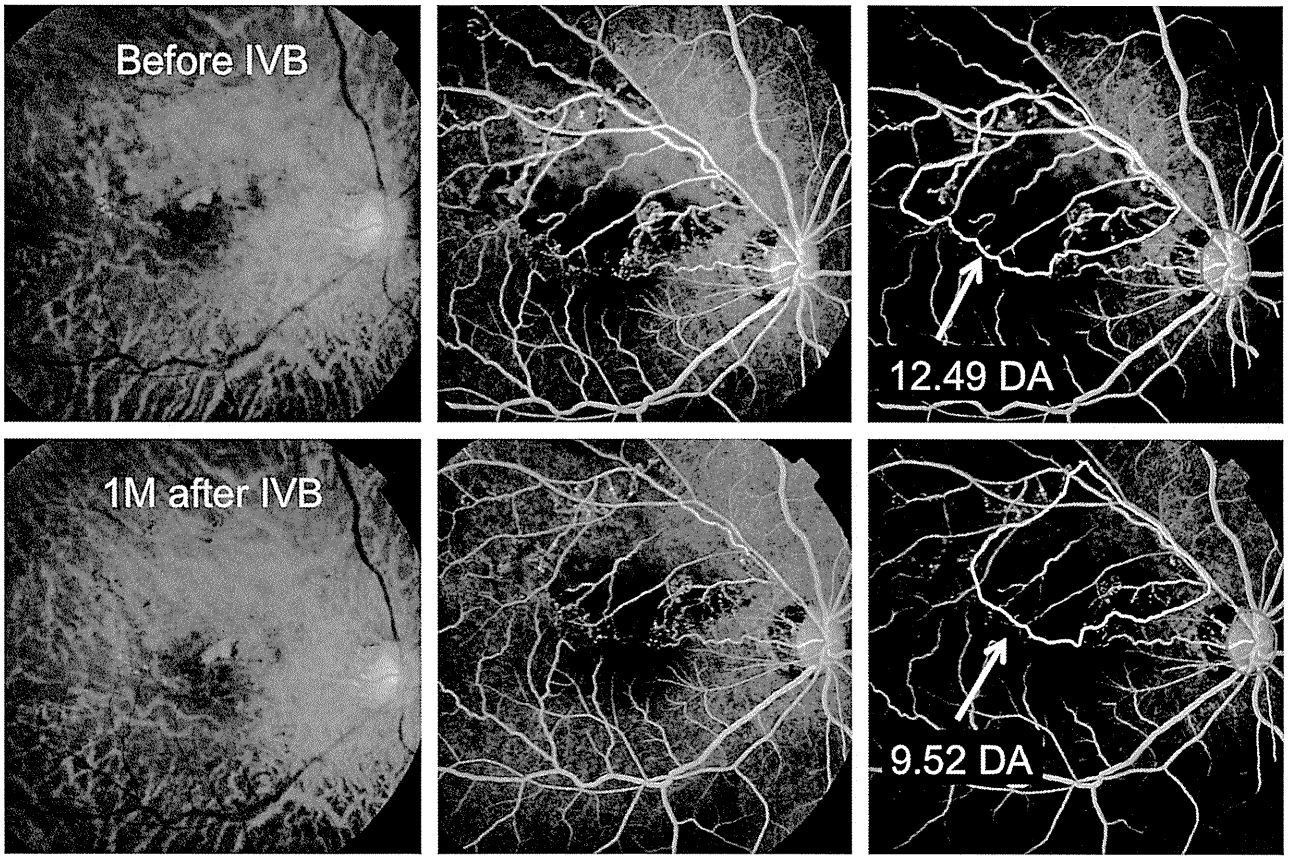

Fig. 3. Fundus photographs and FAs before and 1 month after the IVB in a patient with BRVO (Patient 47, 61-year-old man). The results of the measure of capillary nonperfusion are shown in the right column. The area of nonperfusion decreased from 12.49 DA to 9.52 DA after the IVB.

after the VEGF injection. Based on these results, they suggested that a sudden drop in the VEGF concentration may be responsible for the closure of the normal capillaries. The incidence of severe progression of capillary nonperfusion after the IVB was higher in their animals (80%) than that of our study (1.7%). This difference may be because of the difference in the species and/or degree of retinal ischemic condition before the IVB. When compared with the human BRVO retina, the retina of rabbit neovascularization model shows more severe ischemic changes in which the neovascular membrane develops within 1 week.

There have been recent case reports that showed rapid ischemic changes,[34,35] multiple retinal hemorrhages,[36] and retinal artery occlusion[37] after the IVB therapy. Kim et al[34] reported a case of nonischemic central retinal vein occlusion, which transformed to severe ischemic central retinal vein occlusion 3 weeks after IVB. However, it is questionable whether these rapid ischemic changes are related to the IVB because such changes can occur even during the natural course of retinal vein occlusion. Hayreh et al[42] reported that the incidence of conversion of nonischemic to ischemic central retinal vein occlusion within 6 months was 13.2% in patients aged ≥65 years.

There are four limitations in this study. The first limitation was the lack of control subjects. Without the control subjects, we cannot conclude whether the incidence of severe ischemic changes seen after IVB (1.7%) was really because of the blockage of VEGF or spontaneous changes during the natural course of BRVO. The second limitation was the difficulty in identifying the exact area of capillary nonperfusion for some patients with BRVO. We did not set any observational period before the IVB therapy and started the IVB at a relatively early stage, a mean period from the onset to the injection of 11.1 weeks. At this early stage of BRVO, the extensive blockage because of the retinal hemorrhage often makes the exact measurement of the nonperfused retinal area difficult. The third limitation was that we could not measure the area of peripheral nonperfused retina exactly using our standard fundus camera system. The recently developed ultra wide-field scanning laser ophthalmoscopy combined with a digital area measurement program may be useful in measuring the area

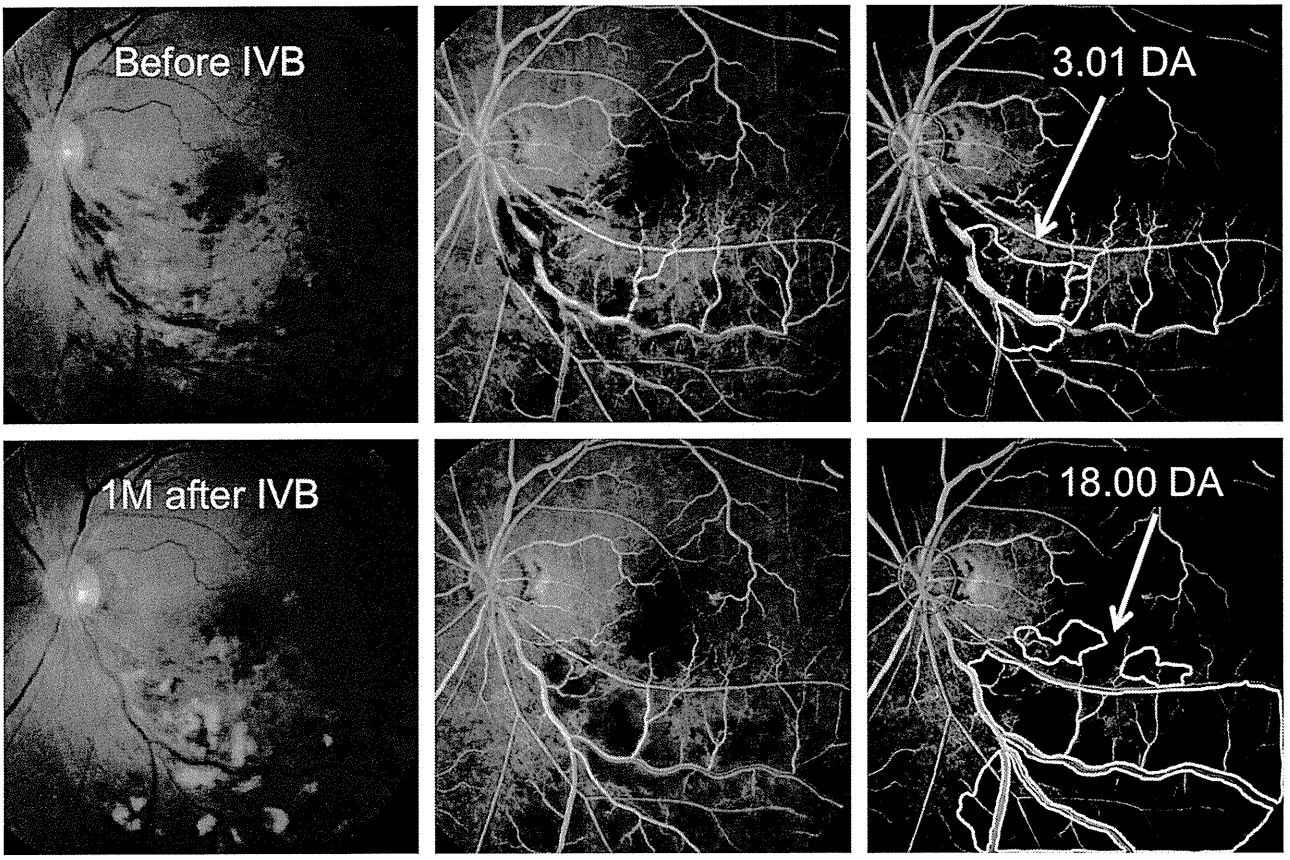

Fig. 4. Fundus photographs and FAs before and 1 month after the IVB in a patient with BRVO (Patient 23, 62-year-old woman). The results of the measure of capillary nonperfusion are shown in the right column. The area of nonperfusion increased from 3.01 DA to 18.00 DA after the IVB, and multiple cotton wool spots developed in the fundus photograph.

of all nonperfused retinas explicitly. The fourth limitation was the small sample size. While the number of eyes treated in this study may be sufficient to rule out a large risk, a much larger sample size would be necessary to rule out a smaller risk or an infrequent complication.

In conclusion, our results demonstrated that the incidence of a significant increase (>1.0 DA) in the area of capillary nonperfusion within 1 month after the IVB was very low (1.7%) in our 58 eyes with BRVO. Furthermore, randomized controlled trials and longer follow-up are needed to clarify whether the IVB therapy exacerbates the retinal ischemia.

Key words: branch retinal vein occlusion, bevacizumab, vascular endothelial growth factor, capillary nonperfusion, ischemia.

Acknowledgment

The authors thank Prof. Duco Hamasaki, Bascom Palmer Eye Institute, Miami, FL, for his critical discussion of the final manuscript.

References

1. Leung DW, Cachianes G, Kuang WJ, Goeddel DV, Ferrara N. Vascular endothelial growth factor is a secreted angiogenic mitogen. Science 1989;246:1306–1309.
2. Keck PJ, Hauser SD, Krivi G, et al. Vascular permeability factor, an endothelial cell mitogen related to PDGF. Science 1989;246:1309–1312.
3. Ferrara N. Vascular endothelial growth factor. The trigger for neovascularization in the eye. Lab Invest 1995;72:615–618.
4. Adamis AP, Shima DT. The role of vascular endothelial growth factor in ocular health and disease. Retina 2005;25:111–118.
5. Shima DT, Adamis AP, Ferrara N, et al. Hypoxic induction of endothelial cell growth factors in retinal cells: identification and characterization of vascular endothelial growth factor (VEGF) as the mitogen. Mol Med 1995;1:182–193.
6. Aiello LP. Clinical implications of vascular growth factors in proliferative retinopathies. Curr Opin Ophthalmol 1997;8: 19–31.
7. Witmer AN, Vrensen GF, Van Noorden CJ, Schlingemann RO. Vascular endothelial growth factors and angiogenesis in eye disease. Prog Retin Eye Res 2003;22:1–29.
8. Campochiaro PA. Seeing the light: new insights into the molecular pathogenesis of retinal diseases. J Cell Physiol 2007; 213:348–354.
9. Sone H, Okuda Y, Kawakami Y, et al. Vascular endothelial growth factor level in aqueous humor of diabetic patients with

rubeotic glaucoma is markedly elevated. Diabetes Care 1996; 19:1306–1307.
10. Ambati J, Chalam KV, Chawla DK, et al. Elevated gamma-aminobutyric acid, glutamate, and vascular endothelial growth factor levels in the vitreous of patients with proliferative diabetic retinopathy. Arch Ophthalmol 1997;115:1161–1166.
11. Clermont AC, Aiello LP, Mori F, Aiello LM, Bursell SE. Vascular endothelial growth factor and severity of nonproliferative diabetic retinopathy mediate retinal hemodynamics in vivo: a potential role for vascular endothelial growth factor in the progression of nonproliferative diabetic retinopathy. Am J Ophthalmol 1997;124:433–446.
12. Sonmez K, Drenser KA, Capone A Jr, Trese MT. Vitreous levels of stromal cell-derived factor 1 and vascular endothelial growth factor in patients with retinopathy of prematurity. Ophthalmology 2008;115:1065–1070.
13. Sato T, Kusaka S, Shimojo H, Fujikado T. Vitreous levels of erythropoietin and vascular endothelial growth factor in eyes with retinopathy of prematurity. Ophthalmology 2009;116: 1599–1603.
14. Nonobe NI, Kachi S, Kondo M, et al. Concentration of vascular endothelial growth factor in aqueous humor of eyes with advanced retinopathy of prematurity before and after intravitreal injection of bevacizumab. Retina 2009;29:579–585.
15. Boyd SR, Zachary I, Chakravarthy U, et al. Correlation of increased vascular endothelial growth factor with neovascularization and permeability in ischemic central vein occlusion. Arch Ophthalmol 2002;120:1644–1650.
16. Noma H, Funatsu H, Yamasaki M, et al. Pathogenesis of macular edema with branch retinal vein occlusion and intraocular levels of vascular endothelial growth factor and interleukin-6. Am J Ophthalmol 2005;140:256–261.
17. Park SP, Ahn JK, Mun GH. Aqueous vascular endothelial growth factor levels are associated with serous macular detachment secondary to branch retinal vein occlusion. Retina 2010;30:281–286.
18. Tong JP, Chan WM, Liu DT, et al. Aqueous humor levels of vascular endothelial growth factor and pigment epithelium-derived factor in polypoidal choroidal vasculopathy and choroidal neovascularization. Am J Ophthalmol 2006;141:456–462.
19. Chan WM, Lai TY, Chan KP, et al. Changes in aqueous vascular endothelial growth factor and pigment epithelial-derived factor levels following intravitreal bevacizumab injections for choroidal neovascularization secondary to age-related macular degeneration or pathologic myopia. Retina 2008;28:1308–1313.
20. Pieramici DJ, Rabena MD. Anti-VEGF therapy: comparison of current and future agents. Eye 2008;22:1330–1336.
21. Klettner A, Roider J. Treating age-related macular degeneration - interaction of VEGF-antagonists with their target. Mini Rev Med Chem 2009;9:1127–1135.
22. Rosenfeld PJ, Brown DM, Heier JS, et al; MARINA Study Group. Ranibizumab for neovascular age-related macular degeneration. N Engl J Med 2006;355:1419–1431.
23. Kondo M, Kondo N, Ito Y, et al. Intravitreal injection of bevacizumab for macular edema secondary to BRVO: results after 12-months and multiple regression analysis. Retina 2009; 29:1242–1248.
24. Rouvas A, Petrou P, Ntouraki A, Douvali M, Ladas I, Vergados I. Intravitreal ranibizumab (Lucentis) for branch retinal vein occlusion-induced macular edema: nine-month results of a prospective study. Retina 2010;30:893–902.
25. Gregori NZ, Rattan GH, Rosenfeld PJ, et al. Safety and efficacy of intravitreal bevacizumab (Avastin) for the management of branch and hemiretinal vein occlusion. Retina 2009;29: 913–925.
26. Avery RL, Pearlman J, Pieramici DJ, et al. Intravitreal bevacizumab (Avastin) in the treatment of proliferative diabetic retinopathy. Ophthalmology 2006;113:1695.e1–e15.
27. Kusaka S, Shima C, Wada K, et al. Efficacy of intravitreal injection of bevacizumab for severe retinopathy of prematurity: a pilot study. Br J Ophthalmol 2008;92:1450–1455.
28. Shord SS, Bressler LR, Tierney LA, Cuellar S, George A. Understanding and managing the possible adverse effects associated with bevacizumab. Am J Health Syst Pharm 2009; 66:999–1013.
29. Prager F, Michels S, Kriechbaum K, et al. Intravitreal bevacizumab (Avastin) for macular oedema secondary to retinal vein occlusion: 12-month results of a prospective clinical trial. Br J Ophthalmol 2009;93:452–456.
30. Kook D, Wolf A, Kreutzer T, et al. Long-term effect of intravitreal bevacizumab (Avastin) in patients with chronic diffuse diabetic macular edema. Retina 2008;28:1053–1060.
31. Neubauer AS, Kook D, Haritoglou C, et al. Bevacizumab and retinal ischemia. Ophthalmology 2007;114:2096.
32. Papadopoulou DN, Mendrinos E, Mangioris G, Donati G, Pournaras CJ. Intravitreal ranibizumab may induce retinal arteriolar vasoconstriction in patients with neovascular age-related macular degeneration. Ophthalmology 2009;116:1755–1761.
33. Ameri H, Chader GJ, Kim JG, Sadda SR, Rao NA, Humayun MS. The effects of intravitreous bevacizumab on retinal neovascular membrane and normal capillaries in rabbits. Invest Ophthalmol Vis Sci 2007;48:5708–5715.
34. Kim KS, Chang HR, Song S. Ischaemic change after intravitreal bevacizumab (Avastin) injection for macular oedema secondary to non-ischaemic central retinal vein occlusion. Acta Ophthalmol 2008;86:925–927.
35. Sabet-Peyman EJ, Heussen FM, Thorne JE, Casparis H, Patel SJ, Do DV. Progression of macular ischemia following intravitreal bevacizumab. Ophthalmic Surg Lasers Imaging 2009;40: 316–318.
36. Lee CS, Koh HJ. Multiple retinal haemorrhages in diabetic retinopathy after adjunctive intravitreal bevacizumab (Avastin) with pars plana vitrectomy. Acta Ophthalmol 2008;86:812–813.
37. von Hanno T, Kinge B, Fossen K. Retinal artery occlusion following intravitreal anti-VEGF therapy. Acta Ophthalmol 2010;88:263–266.
38. Takahashi K, Kishi S, Muraoka K, Shimizu K. Reperfusion of occluded capillary beds in diabetic retinopathy. Am J Ophthalmol 1998;126:791–797.
39. Ishikawa K, Kondo M, Ito Y, et al. Correlation between focal macular electroretinograms and angiographic findings after photodynamic therapy. Invest Ophthalmol Vis Sci 2007;48: 2254–2259.
40. Sugita T, Kondo M, Piao CH, Ito Y, Terasaki H. Correlation between macular volume and focal macular electroretinogram in patients with retinitis pigmentosa. Invest Ophthalmol Vis Sci 2008;49:3551–3558.
41. Costa RA, Calucci D, Skaf M, et al. Optical coherence tomography3: automatic delineation of the outer neural retinal boundary and its influence on retinal thickness measurements. Invest Ophthalmol Vis Sci 2004;45:2399–2406.
42. Hayreh SS, Zimmerman MB, Podhajsky P. Incidence of various types of retinal vein occlusion and their recurrence and demographic characteristics. Am J Ophthalmol 1994;117:429–441.
43. Rehak J, Rehak M. Branch retinal vein occlusion: pathogenesis, visual prognosis, and treatment modalities. Curr Eye Res 2008;33:111–131.

GANKA. OPHTHALMOLOGY Vol. 53 No. 10 2011

眼　科

臨時増刊号：眼科最新手術

顕微鏡による新しい観察システム

門之園一明

金原出版株式会社

毒性も軽減できる可能性があるなどの利点が多い[8]。しかし，大量の硝子体出血を認める症例にシャンデリア照明を用いる場合，まれに照明ファイバーの先端に凝血塊が付着し，それに伴う吸熱反応が原因でファイバー先端に熱溶解を生じることがある[9]。このような懸念がある症例では手術開始時に照明ファイバー先端部周囲の硝子体を先に切除してしまうと良い。また，シャンデリア照明ファイバーは空気灌流下でもその先端が高熱となることが知られており，液・空気置換後は光量を下げることや必要以上に長時間にわたって空気灌流下で使用しないなどの対処が必要である。

Ⅲ 今後の展望

キセノンや水銀蒸気灯のような低出力かつ高輝度の照明を実現できる光源を用いた照明装置は，今後の眼内照明ファイバーのサイズやバリエーションの開発のニーズに応えるべく，従来のハロゲンライト光源にとって代わり，硝子体手術照明の主役になることに疑う余地はない。実際のところ，次世代の硝子体手術装置として最近発売されたAlcon社のConstellation®やBausch & Lomb社のStellaris PC®のいずれもキセノン光源や水銀蒸気灯が内蔵の照明光源として標準装備されている。

これらの新しい光源装置，眼内照明と次世代の硝子体手術装置を組み合わせることによって，今後の小切開硝子体手術のシステム開発はさらに低侵襲な方向に向かって発展することは間違いないであろう。

文献

1) Oshima Y et al : Self-retaining 27-gauge transconjunctival chandelier endoillumination for panoramic viewing during vitreous surgery. Am J Ophthalmol 143 : 166-167, 2007
2) Oshima Y et al : Novel mercury vapor illuminator combined with a 27/29-gauge chandelier light fiber for vitreous surgery. Retina 28 : 171-173, 2008
3) Eckardt C et al : 27-gauge Twinlight chandelier illumination system for bimanual transconjunctival vitrectomy. Retina 28 : 518-519, 2008
4) 大島佑介：ニューインスルメント：硝子体手術用キセノン光源装置とシャンデリア方式の眼内照明．眼科手術 18 : 515-518, 2005
5) 若林 卓ほか：ニューインスルメント：経結膜無縫合硝子体手術における新しいシャンデリア方式の眼内照明．眼科手術 20 : 61-65, 2007
6) 若林 卓ほか：ニューインスルメント：水銀光源装置(Photon II™)．眼科手術 20 : 497-500, 2007
7) Sakaguchi H et al : A 29/30-gauge dual chandelier illumination system for panoramic viewing during microincision vitrectomy surgery. Retina(in press)
8) van den Biesen PR et al : Endoillumination during vitrectomy and phototoxicity thresholds. Br J Ophthalmol 84 : 1372-1375, 2000
9) Shimada H et al : Thermal injury caused by chandelier fiber probe. Am J Ophthalmol 143 : 167-169, 2007

8 顕微鏡による新しい観察システム

はじめに

硝子体手術においてクリアな観察系は最も重要な手術の成功のカギである。顕微鏡手術においては，非接触広角観察システムが近年の硝子体手術の術中観察系において注目される顕微鏡による手術観察システムである。広角観察システムには，非接触と接触があり，非接触はBIOM，OFF-ISS，Resightの3種類の機種が主に本邦でよく使用されている(表)。また，それぞれの機種には独自の広角観察画像を得る工夫が施されている。本稿では，主に最近話題となっている非接触広角観察システム，Resight (Lumera 700，Zeiss)についてその概略を説明する。

I 広角観察システム手術顕微鏡

非接触レンズにより術者は，広角の眼底画像を得ることができるが，その画像は反転している。このため，広角観察系を硝子体手術中に用いるためには画像を正立像にする必要があり，手術顕微鏡に取り付けられた画像反転装置(SDIと呼ばれる)により，術者は正立像として術野を認識して手術を遂行することが可能である。

一般に，レンズを角膜面上に近付けることにより得られる眼底画像はより広角になり，その焦点は角膜面上に近くなる。一方，レンズを遠ざけることにより得られる眼底画像は狭く，その焦点は網膜面上に近くなる。すなわち，接触レンズの移動のみでは，的確な広角画像を得ることはできない(図1)。このため，従来は術中の広角画像の焦点合わせの習得が非常に難しく，広角観察系は，

表

製造元	Carl Zeiss Meditec		OCULUS		TOPCON	
名称	Resight		BIOM 4e		OFFISS	
レンズディオプター(D)	60	128	60	120	40	120
レンズ自体の径	17 mm		19 mm		25 mm	21 mm
レンズ枠を含めた径	20 mm		20 mm		28 mm	23.5 mm
取付可能な顕微鏡	Zeiss社製のLumera 700，Lumera T，VISU 210，VISU 200など		ほぼすべての顕微鏡(Zeiss，Leica，Topcon)		トプコン社OMS-800，850のみ	
像の見え方	倒像		倒像		倒像	
追加のインバーター	不要(電動インバーター鏡筒)		必要(SDI)		必要(SDI)	
追加のフットスイッチ	不要		必要(Zeissとの組み合わせの場合)		不要	

門之園一明
Kazuaki KADONOSONO 横浜市立大学附属市民総合医療センター眼科

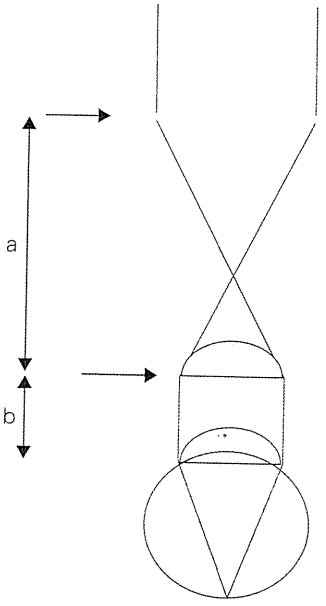

図1：広角観察システムの光学的特徴

顕微鏡の接眼レンズ（上の矢印）と非接触レンズ（下の矢印）との距離（a）および非接触レンズと角膜面との距離（b）が眼底に対する焦点合わせに関連する。主にBIOMで用いられている。

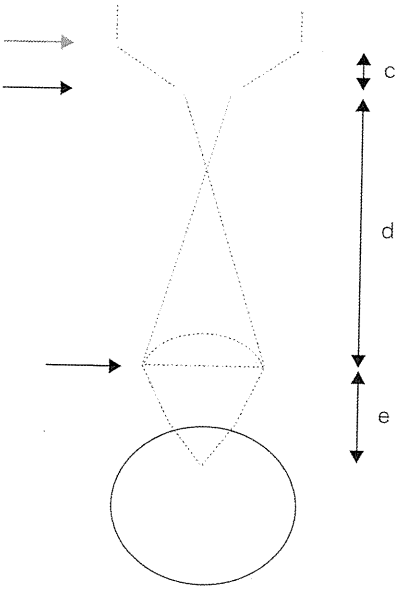

図2：内部焦点合わせを用いた広角観察システムの光学的特徴

焦点は顕微鏡鏡筒内の内部レンズ（赤矢印），および顕微鏡の接眼レンズ（上の矢印）と非接触レンズ（下の矢印）との距離（c）および非接触レンズと角膜面との距離（d）により決定される。焦点合わせは，内部レンズの上下移動により簡便に行われる。Resight手術顕微鏡において用いられる。角膜面上と非接触レンズとの距離（e）は一定である。

接触レンズに比較して劣っていると考えられてきた。結果的にわが国では，硝子体手術においては，より簡便である接触レンズが広く使用され，歴史的に欧米と異なり広角観察システムは十分な普及をみることはなかった。ところが，近年使用が可能となったResight（Lumera 700）は，reduction lensを顕微鏡鏡筒内に内蔵することで，焦点合わせを広角合わせと独立して行うことを可能とした（図2）。このため，術者は，適切な画角で，適切な対象物を手術中に簡便に確認することができるようになった（図3）。

眼科手術にとって，観察対象物の奥行きは眼球の大きさを考慮すると，2〜3 cm程度と非常に小さい。このため，眼科手術顕微鏡では，従来より焦点合わせ（focus）は対物レンズの上下移動により行われてきた。一方，脳神経外科など手術対象物の奥行きが広く，手術中の出血などによるレンズへの損傷が生じる可能性のある臓器を扱う分野では，焦点合わせは顕微鏡の上下移動ではなく，内部レンズの上下移動による焦点合わせシステムにより行われていた。すなわち，顕微鏡本体と対象物との距離は変わらない。Resightは，従来より他科手術顕微鏡で使用されていたこの内部焦点システムを眼科顕微鏡に初めて応用した。このアイデアは，結果的に広角でかつ的確な焦点合わせ（focus）機能を可能とした。

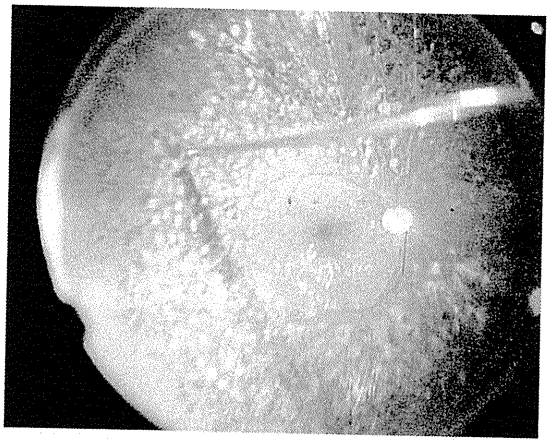

図3：広角観察システムによる眼底画像

ほぼ周辺部網膜まで網膜は広く観察される。また，光凝固を施行している網膜の画像に焦点は良く合っている。

問題点：非接触レンズ広角観察システムでは，前置レンズの曇りおよび器具との干渉が問題になる(図4)。また，レンズ固定の支持バーのずれにより術野のずれが生じることがある。

Ⅱ 広角観察システムの応用例

1 症例1

67歳の男性で7年前に白内障手術を受けた。数日前に突然の視力障害をきたし来院した。眼底検査で，眼内レンズの眼底への落下が観察され眼内レンズの摘出術を受けた。図5は，手術中の眼内レンズが液体パーフルオロカーボン(PFC)上に浮かび注入に伴い眼内レンズが角膜側に移動してきている手術画像である。ここで注目すべきは，周辺部の網膜の状態を確認しつつ，落下した眼内レンズを観察し続けることがこの広角顕微鏡システムでは可能なことである。眼内レンズは，PFC上で氷の上のようにつるつると移動し術野の死角に入る可能性がある。このため，眼内レンズをPFCで摘出する場合は，周辺部網膜を確認することが重要となる。広角観察手術顕微鏡は，このような症例には有用である。その後，眼内レンズは首尾よく摘出され術後視力は矯正1.0まで回復した。

図4：問題点

非接触128°レンズは角膜上約1.0～1.5 mm程度の前方ある。このため，しばしばレンズの曇りおよび硝子体器具が操作の際にレンズに当たる。

2 症例2

53歳の女性，術前視力は手動弁であった。網膜剝離手術後の再剝離の症例であった。眼底は，視神経乳頭が閉じている漏斗状の増殖硝子体網膜症(PVR)であり，ナプキンリングと呼ばれる網膜下増殖の存在も確認された。本症例に対して硝子体手術が行われ，増殖膜が除去された。図6は，広角観察手術顕微鏡を用いた術中画像である。膜剝離のための硝子体鑷子の先端は網膜面上の増殖膜にあり，かつそれと同時に周辺部網膜は十分に確認可能である。このようなPVR症例では，増殖膜の処理に気を取られしばしば周辺部の異変に気づくことが遅れることがある。広くかつ良好な術野を得ることで，PVR手術に伴う網膜

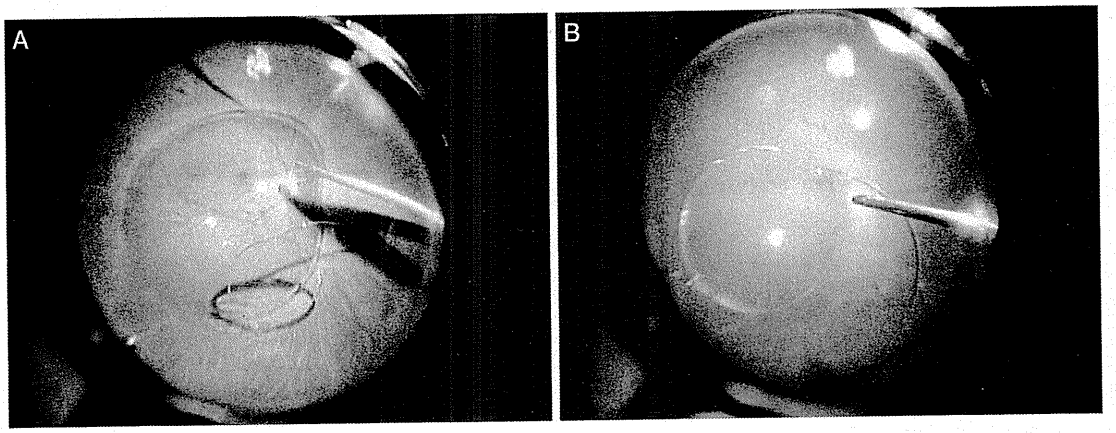

図5：落下眼内レンズの眼底画像

パーフルオロカーボンを注入して眼内レンズを浮揚させている。ほぼ周辺部網膜まで観察される(A)。また，眼内レンズはよく確認されかつほぼ赤道部網膜まで観察される(B)。

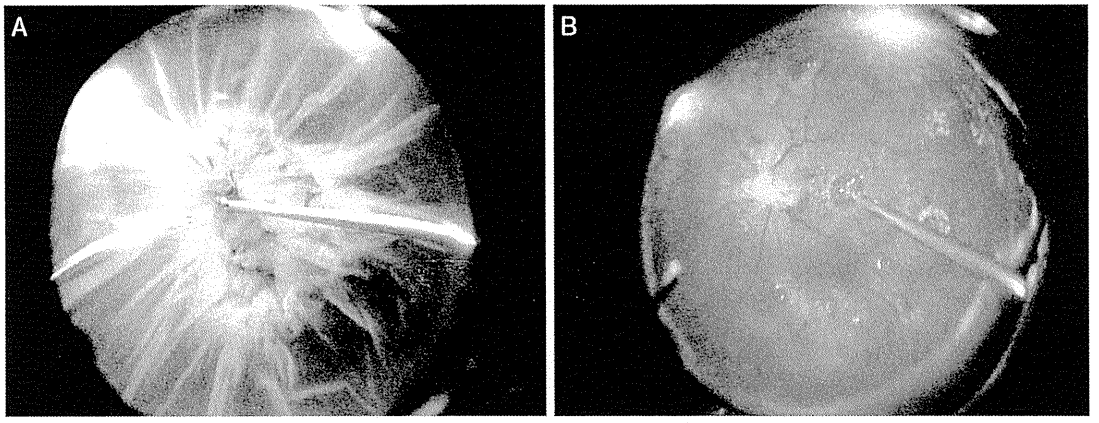

図 6：増殖硝子体網膜症の硝子体手術術野画像

全剥離した周辺部網膜が確認される。また，鑷子にて増殖膜の切除がよく観察される(A)。その後，網膜はよく復位されパーフルオロカーボンの粒子をフルートニードルにて受動吸引しているのがよく観察され，同時に眼底にシリコーンオイルがほぼ充填されつつあるのがよくわかる(B)。

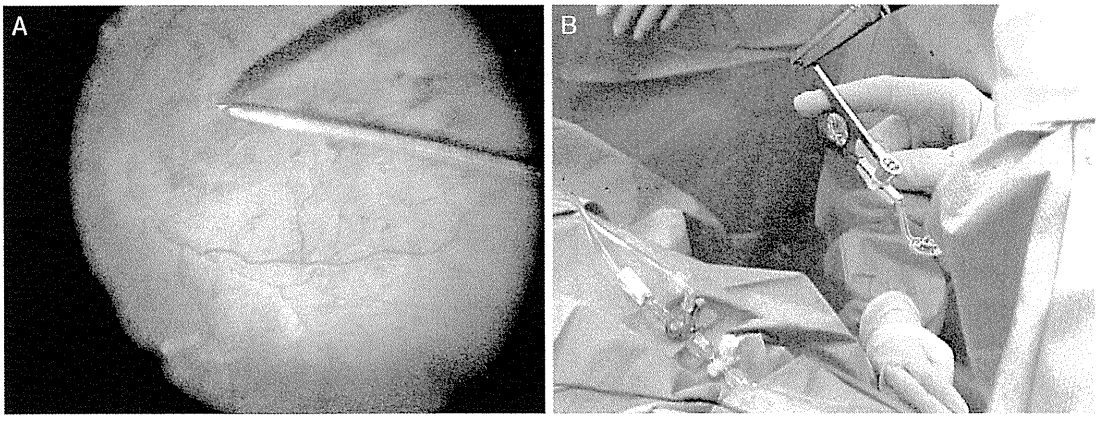

図 7：黄斑円孔の内境界膜剥離

広角観察システムを用いているが後極部網膜をよく観察できる。内境界膜は非接触レンズでもよく確認できる(A)。手術中に簡便に Resight 手術顕微鏡の 60°非接触レンズを使用することが可能である(B)。

裂孔や出血などの合併症は軽減することができる。

また，PFC は，多くの場合最終的に術中にシリコーンオイルへ置換される。PFC-シリコーンオイル置換において重要なことは，PFC の粒子を見失わないことと，周辺部網膜にシリコーンオイルの注入過程にて異変がないか否かを確認することである。さらに，視神経乳頭の色調の変化を確認することも重要である。このため，手術中に広角かつ的確な画像を得ることは安全なシリコーンオイル置換術にとって重要であり，広角観察システムの利点が生かされる症例である。

症例 3

56 歳の男性，黄斑円孔の患者である。黄斑円孔に対する硝子体手術が行われた。図 7A は内境界膜剥離を行っている術中写真である。通常この繊細な手技は，接触レンズ下に行われていたが，Resight 手術顕微鏡では，非接触レンズのまま，内境界膜を剥離することが可能である。60°レンズを使用することで(図 7B)，染色された内境界膜を剥離することが可能となる。従来，広角観察システムの欠点として黄斑部網膜の処理を行うことができない点が挙げられていたが，Reisght 手術顕微鏡では，広角観察システムと同時に黄斑部

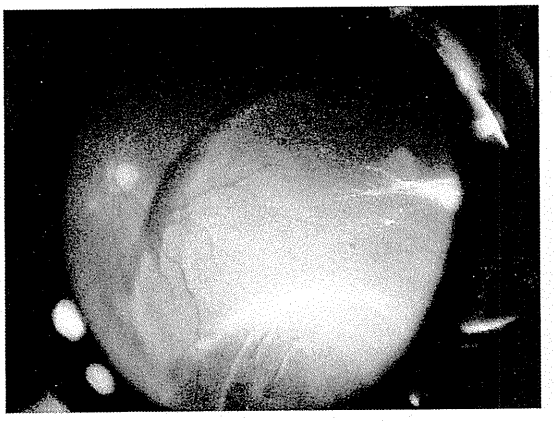

図 8：強膜内陥術

広角観察システムにより，萎縮性円孔に対する網膜冷凍凝固がより的確に簡便にできる。

治療を行うことができる。

症例 4

28 歳の男性。萎縮性円孔を原因とする裂孔原性網膜剝離に対する強膜内陥術を施行された（図 8）。Resight 手術顕微鏡により，術中のバックリング操作を顕微鏡下で行うことが可能である。

まとめ

近年，硝子体手術において広角観察手術顕微鏡は急速に普及しつつある。さまざまな種類の広角観察手術顕微鏡が市販されている。なかでも，内部焦点をもつ手術顕微鏡は，広角かつクリアな術野という相反する事象を具現化した。今後，本邦でも欧米のように，硝子体手術の観察系は広角へとシフトしてゆくと予想される。それは，硝子体手術の治療成績をさらに進歩させるであろう。

An Experimental Study of Retinal Endovascular Surgery with a Microfabricated Needle

Kazuaki Kadonosono,[1] *Akira Arakawa,*[1] *Shin Yamane,*[1] *Eiichi Uchio,*[2] *and Yasuo Yanagi,*[3]

Purpose. To study the feasibility of performing retinal endovascular surgery with a microfabricated needle-based cannulation system at the level of the retinal microvasculature.

Methods. A total of 40 retinal vein vessels, and 40 porcine eyes were used, and the eyecups were prepared under an operating microscope. Twenty retinal veins each were pierced with a microfabricated needle having an outer diameter of 50 μm and with a micropipette having an outer diameter of 50 μm, respectively, and each vessel that was successfully pierced was injected with a solution. The piercing success rates and injection success rates were calculated, and a histologic examination of the site was performed in each eye.

Results. Piercing and injection with the microneedle were successful in all 20 eyes (100%). Histologic examination showed that the retinal vasculature was well preserved in all eyes in which piercing had been performed with the microneedle. Piercing with the micropipette, on the other hand, was successful in only 8 eyes (40%), and injection with the micropipette was successful in only 5 eyes (25%). The tip of the micropipette broke in 12 vessels during piercing and in 3 vessels during injection.

Conclusions. The feasibility of performing microvascular piercing and intravascular injection of retinal veins with a microneedle was demonstrated in porcine eyes. It may be possible to administer solutions into retinal vessels more effectively with a microfabricated needle, and that may contribute to improving retinal endovascular surgery in human eyes. (*Invest Ophthalmol Vis Sci.* 2011;52:5790-5793) DOI:10.1167/iovs.11-7327

Because retinal vascular occlusions may be initiated by endovascular pathophysiologic mechanisms,[1,2] endovascular surgery has been considered as a potential treatment. However, despite several earlier intensive experimental and clinical studies, this surgical approach has never become completely established.[3-11] Retinal vein cannulation is one of the surgical procedures that are performed on the retinal vasculature.[12,13] It involves puncture, injection, and cannulation, and has been performed in studies on both animal and human eyes. However, several problems related to the surgical technique remain in retinal endovascular surgery, and as a result it is still challenging and has never been evaluated as useful clinically.[14-19]

Glass micropipettes have been produced with very fine tips and diameters that enabled them to be used for such applications as pressure injection, ion sensing, and microvascular puncture.[20] Glass micropipettes are so sharp that they easily pierce the retinal microvasculature, and thus have been considered the most suitable surgical tools for retinal endovascular surgery.[3-13] However, micropipettes have the disadvantage of being so frangible and delicate that it is difficult to maneuver them during cannulation procedures on retinal vessels.

In recent years, microneedles have been fabricated by leveraging tools from the microelectronics industry, and they have been assessed as devices to facilitate administration delivery.[21-23] Because fabricated microneedles may be sharp and rigid enough to serve as tools for microvascular surgery, we compared the performance of microneedles and conventional micropipettes as a means of cannulating and injection of retinal veins in porcine eyes.

Materials and Methods

Porcine Eyes

More than 40 porcine eyes were prepared for use in this study. The eyes were delivered fresh, and they were used within 24 hours of enucleation. All maneuvers were performed on the eyecup in room air. The anterior segment was excised by circumferential incision at the level of the pars plana. The vitreous was removed by the en bloc method, which exerts minimal traction on the retinal surface. The vitreous base was gently massaged with a dry cotton-tipped applicator until it separated from the vitreous base, making it possible to remove and roll the vitreous out of the eye en bloc with the applicator. The residual fluid on the retinal surface was aspirated with a blunt 30-gauge cannula. All procedures were approved by the institutional animal care and use committee of Yokohama City University Medical Center and complied with the ARVO Statement for the Use of Animals in Ophthalmic and Vision Research.

Preparation of the Microneedles

An application-independent optimal design for the microneedle was prepared. The microfabricated needles were manufactured to be angled and jointed with an angled 23-gauge steel pipe (Medical Planning Laboratory Ltd., Tochigi, Japan) (Figs. 1 and 2). In general, needles having a smaller diameter made of stainless steel are sharper and can withstand higher pressure without fracturing or buckling. On the other hand, the flow rate through microneedles declines as their diameter decreases, and the pressure increases. With this in mind, the outer micrometer size domain of the microneedle was designed to be 40 to 50 μm, because the diameter of first-order retinal veins in human eyes is approximately 100 μm.[24]

Also, because needles with a steep angled cutting plane at the tip, whose angle from the axis of the needle shaft is greater than 60°, are sharper and capable of piercing the microvasculature more smoothly, the cutting plane of the needle was designed to have a 30° angle, i.e.,

From the [1]Department of Ophthalmology, Yokohama City University Medical Center; [2]Department of Ophthalmology, Fukuoka University School of Medicine; and [3]Department of Ophthalmology, University of Tokyo School of Medicine.

Submitted for publication February 4, 2011; revised May 9 and 19, 2011; accepted May 24, 2011.

Disclosure: **K. Kadonosono**, None; **A. Arakawa**, None; **S. Yamane**, None; **E. Uchio**, None; **Y. Yanagi**, None

Corresponding author: Kazuaki Kadonosono, Department of Ophthalmology, Yokohama City University, 4-57 Urafune-cho Minami-ku, Yokohama 232-0024, Japan; kado@med.yokohama-cu.ac.jp.

Investigative Ophthalmology & Visual Science, July 2011, Vol. 52, No. 8

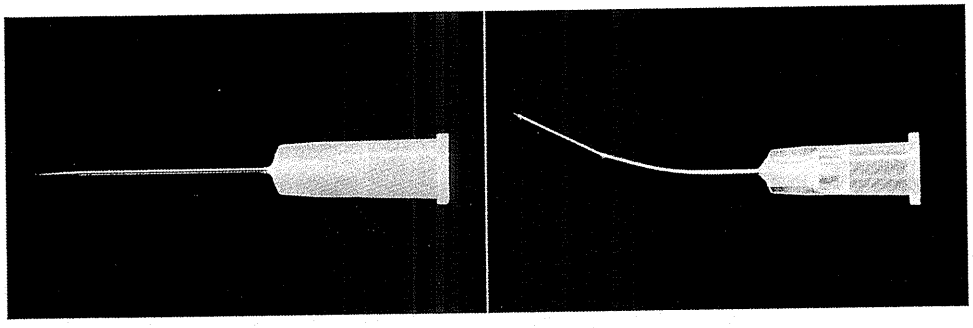

FIGURE 1. Photograph of a microfabricated needle and a micropipette. *Left:* The micropipette. Glass tubes 26 mm in length having an outer diameter of 50 μm and a 30° angle tip were designed to be attached to a 23-gauge cannula. *Right:* The microfabricated needle. The microneedle was manufactured with a curved shaft attached to a 23-gauge holder. The outer micrometer size domain of the microneedle was designed to be 50 μm, and the length of the front of the needle was designed to be 1.5 mm.

60° angle from the axis of the needle shaft (Fig. 3). Shorter needles of the same diameter and material can withstand higher pressures without fracturing or buckling. Lower microneedle height allows cannulation of smaller needle diameters without inducing buckling. A smaller tip diameter results in a much higher ratio of fracture force to insertion force into the microvasculature. Accordingly, the front of the microneedle was designed to be 1.5 mm long and to be connected to a 23-gauge needle. A photograph of the microneedle is shown in Figures 1 and 2.

Preparation of the Micropipettes

Micropipettes were prepared and manufactured from unsharpened standard glass pipettes (Primetech Laboratory Ltd, Ibaragi, Japan). Glass tubes 26 mm in length having an outer diameter of 50 μm with a 30° angle tip were designed to be attached to a 23-gauge cannula (Figs. 1 and 2).

Piercing and Injection

Retinal veins were punctured at a site near the optic nerve head where the diameter of the vein was maximal and the vein was tightly tethered to the optic nerve head. The vein was injected with balanced saline solution (BSS) at high pressure of approximately 50 mm Hg created with a viscous-fluid control machine (Accurus, Alcon, TX), and retrograde blood flow was considered evidence of successful injection of the solution. The flow rate and the inside diameter in the micropipette were approximately 0.077 mL per second and 30 μm, respectively, while those of the microneedle were approximately 0.083 mL per second and 35 μm, respectively. The duration of the injection was three minutes. These procedures were performed manually and the instruments were held with the hands, and there was no significant movement or distortion of the vessels during the procedures. The success rate of piercing and injection with each instrument was evaluated in all procedures, and a histologic examination was performed on all eyes. After successful piercing and injection of the retinal vein, the specimen was preserved and photographed, and the site of the piercing was identified under a microscope. The specimen was then embedded in paraffin, and every section up to a distance of 500 μm from the site of the piercing was mounted. Serial sections were examined to determine the integrity of the retinal vasculature after the piercing.

RESULTS

Piercing and injection were performed with micropipettes and microneedles on a retinal veins in 20 porcine eyes each, and a total of 40 retinal veins in 40 porcine eyes were used (Table 1).

All attempts to pierce the retinal vein with a microneedle were successful. The resistance of the retinal vein to piercing was low, and no microneedles broke as a result of unintentional tremors or movements of the microneedles. After the vein had been pierced, a BSS injection was performed (Fig. 4). Blood flow was clearly observed in all 20 eyes. The success rates of both piercing and injection with the microneedle procedure were 100%.

On the other hand, piercing the retinal vein near the optic nerve with 8 micropipettes was attempted, and then BSS was injected after the piercing procedure in all 8 eyes in which piercing was attempted (Fig. 4). The other 12 micropipettes broke near their tip during the piercing procedure. Thus, the piercing procedure and the injection procedure were both successful with only 5 micropipettes. No blood flow at all was seen or it stopped during the injection in 3 eyes because the

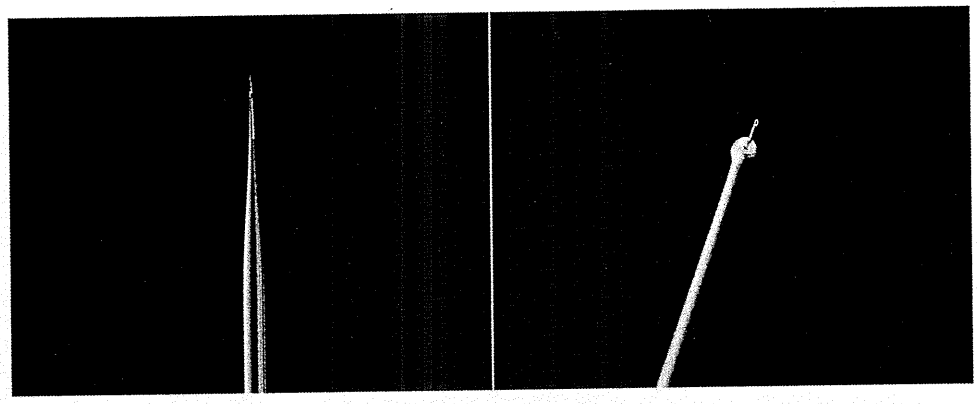

FIGURE 2. Magnified photograph of the tip of the micropipette (*left*) and the microfabricated needle (*right*).